Articles

Stoichiometric CO Reductive Titrations of Acetyl-CoA Synthase (Carbon Monoxide Dehydrogenase) from *Clostridium thermoaceticum*†

Daniel M. Fraser‡ and Paul A. Lindahl*,§

Departments of Chemistry and of Biochemistry and Biophysics, Texas A&M University, College Station, Texas 77842

Received February 18, 1999; Revised Manuscript Received September 17, 1999

ABSTRACT: Acetyl-CoA synthase (carbon monoxide dehydrogenase) from *Clostridium thermoaceticum* was stoichiometrically titrated under CO_2 with CO and thionin. Resulting EPR titration curves were simulated assuming different redox descriptions of the enzyme. Samples began slightly reduced, with ∼20% of the C-cluster reduced to the C_{red1} state. With increasing CO intensities, the intensity of C_{red1} increased to a maximum, and then declined as the intensities of C_{red2}, B_{red}, and A_{red}−CO increased and plateaued. Simulations revealed that only a fraction of the A-, B-, and C-centers in the enzyme were redox-active and that, within the probed potentials (−0.2 to −0.45 V), there are probably no other redox sites in the enzyme. Oxidative processes occurred at higher potentials, but they are catalytically irrelevant. Additional low-potential redox sites may be present, but this could not be assessed from the titrations. Best-fit $E°_{C_{ox}/C_{red1}} = -0.12 \pm 0.04$ V, 0.1 V less negative than under Ar. Titrated samples accepted from 3.5 to 5.0 equiv/$\alpha\beta$ in accordance with the intensity of the sample's EPR signals. A similar titration under Ar revealed a different pattern of reduction. The intensity of B_{red} increased first; then C_{red1} converted to C_{red2}, and then A_{red}−CO developed. The sample accepted ∼4 equiv/$\alpha\beta$. The heterogeneity in the enzyme is summarized as follows. About forty percent of A_{ox} can be reduced by one electron and bound with CO, yielding A_{red}−CO. The remaining A_{ox} cannot be reduced. All B_{ox} can be reduced, most (∼65%) to the $S = {}^1/_2$ state and the remainder to the $S = {}^3/_2$ state. About 40% of C_{ox} are reduced by one electron to C_{red1} and then by two more electrons to C_{red2}. The remaining C_{ox} clusters are reduced by one electron to an $S = {}^3/_2$ form. Possible origins of this heterogeneity are discussed.

Methanogenic archaea and acetogenic bacteria use the Wood/Ljungdahl pathway to grow autotrophically on CO_2 and H_2. Acetyl-CoA synthase (ACS),[1] previously called carbon monoxide dehydrogenase (CODH), is a major enzyme in this pathway (*1*). It catalyzes two reactions, including the reversible reduction of CO_2 to CO (reaction 1)

$$CO_2 + 2e^- + 2H^+ = CO + H_2O \quad (1)$$

and the synthesis of acetyl-CoA from CO, coenzyme A, and a methyl group. In *Clostridium thermoaceticum*, the methyl group is transferred onto ACS from a corrin−iron−sulfur protein (CoFeSP) (reaction 2).

$$CO + CoASH + CH_3{-}Co^{3+}FeSP \rightleftharpoons CH_3{-}C(O){-}SCoA + Co^{+}FeSP + H^+ \quad (2)$$

ACS from *C. thermoaceticum* is an $\alpha_2\beta_2$ tetramer (*2*). Each $\alpha\beta$ dimer houses three metal clusters, called A−C, and possibly additional EPR-silent redox centers. The A-cluster, a Ni−X−Fe_4S_4 cluster (X is an unknown bridge) located in the α-subunit, is the active site for acetyl-CoA synthesis (*3*−*7*). The diamagnetic oxidized A_{ox} state can be reduced by an electron and bound by CO, yielding the A_{red}−CO state. This $S = {}^1/_2$ state exhibits the so-called NiFeC EPR signal ($g = 2.09$, 2.08, and 2.02).

The electron used to reduce the A-cluster typically comes from the oxidation of CO at the C-cluster. The reduction potential and CO binding constant have not been measured independently, but the effective potential for the A_{ox}-to-A_{red}-

† This research was supported by the National Institutes of Health (GM46441) and the Robert A. Welch Foundation (A1170).

* To whom correspondence should be addressed. Telephone: (409) 845-0956. E-mail: Lindahl@chemvx.tamu.edu.

‡ Department of Chemistry.

§ Departments of Chemistry and of Biochemistry and Biophysics.

[1] Abbreviations: ACS, acetyl-CoA synthase (previously carbon monoxide dehydrogenase, abbreviated CODH); C_{ox}, C_{red1}, C_{int}, and C_{red2}, fully oxidized and one-, two-, and three-electron-reduced states of the C-cluster, respectively; A_{ox} and A_{red}−CO, oxidized and one-electron-reduced and CO-bound states of the A-cluster, respectively; B_{ox} and B_{red}, oxidized and one-electron-reduced states of the B-cluster; $E°_{ox/red}$, thermodynamic reduction potentials for various ox/red redox couples; CoFeSP, corrinoid−iron−sulfur protein; CoASH or CoA, coenzyme A; phen, 1,10-phenanthroline; MES, 2-(*N*-morpholino)ethanesulfonic acid; thionin, 3,7-diaminophenothiazin-5-ium chloride; E_{tot}, total enzyme concentration; PPX model, partial-plus-X model describing the redox sites in ACS; PMX model, partial-minus-X model; TPX model, total-plus-X model; TMX model, total-minus-X model.

10.1021/bi990397n CCC: $18.00
Published on Web 11/06/1999

CO transition ($E°_{A_{ox}/A_{red}-CO}$) performed under a CO_2 atmosphere at pH 6.3 is −0.173 V (*8*).[2]

The B- and C-clusters are located in the β-subunit. The B-cluster is an $[Fe_4S_4]^{2+/1+}$ cluster ($E°_{B_{ox}/B_{red}} = -0.366$ V) that transfers electrons between the C-cluster and external redox agents (*9*, *10*). The $S = {}^1/_2$ B_{red} state exhibits an EPR signal ($g = 2.04$, 1.94, and 1.90; $g_{av} = 1.94$), while B_{ox} is diamagnetic (*9*, *10*).

The C-cluster is the active site for CO/CO_2 redox catalysis (*11*−*13*). It also consists of a Ni ion linked to an Fe_4S_4 cluster (*14*). The C-cluster is stable in (at least) three redox states, called C_{ox}, C_{red1}, and C_{red2}. One-electron reduction of the diamagnetic C_{ox} state ($E°_{C_{ox}/C_{red1}} = -0.22$ V under an Ar atmosphere) yields C_{red1}, an $S = {}^1/_2$ EPR-active ($g = 2.01$, 1.80, and 1.64; $g_{av} = 1.82$) state. Further reduction of the enzyme ($E°_{C_{red1}/C_{red2}} = -0.345$ V) yields C_{red2}, another $S = {}^1/_2$ EPR-active ($g = 1.97$, 1.87, and 1.75; $g_{av} = 1.86$) state. Anderson and Lindahl (*12*, *13*) proposed that C_{red2} is two electrons more reduced than C_{red1}, though this is not certain. They also proposed a fourth redox state of the C-cluster, called C_{int}, thought to be one electron more reduced than C_{red1} and one electron more oxidized than C_{red2} (*13*).

Additional EPR-silent redox centers have been suggested. Barondeau and Lindahl proposed that ACS contains a low-potential cystine−cysteine redox site called D (*15*). This hypothetical species is thought to serve as a surrogate electron-transfer agent to maintain the Ni of the A-cluster in the 2+ state at each step of catalysis. $E°_{D_{ox}/D_{red}}$ was estimated to be about −0.53 V under Ar, but the value has not been determined for samples under CO_2. Anderson and Lindahl (*13*) proposed an $n = 1$ redox-active species X to serve as another electron-transfer agent similar to the B-cluster. They stressed that X could be either another redox site in the enzyme or one of the known clusters (A−C) in another ACS molecule. Seravalli et al. (*16*) supported and expanded the idea that X is another redox site in ACS, and concluded that their redox titrations of ACS provided evidence for it. Maupin-Furlow and Ferry (*17*) proposed a second A-cluster in the subunit of ACS from *Methanosarcina thermophilia* that would correspond to the β-subunit of the ACS from *C. thermoaceticum*.

One of the most peculiar properties of ACS is that only about 30−50% of its $\alpha\beta$ dimeric units appear to be catalytically active. The evidence for this is substantial but not definitive. First, all EPR signals described above quantify to substantially less than 1 spin/$\alpha\beta$ (the signals from A_{red}−CO, B_{red}, C_{red1}, and C_{red2} typically quantify to about 0.2, 0.7, 0.3, and 0.3 spin/$\alpha\beta$, respectively) (*9*, *10*). This suggests that only a fraction of clusters are redox-active. Second, the labile Ni of the A-cluster can be selectively removed by 1,10-phenanthroline (phen), eliminating the CO−acetyl-CoA exchange activity (*3*, *4*). However, phen treatment removes only ∼0.3 Ni/$\alpha\beta$ (*18*), suggesting that only a fraction of A-clusters are catalytically active. Third, only about 40% of CO-reduced α-subunits exhibit magnetic Mössbauer features due to the A_{red}−CO state; the remainder yield diamagnetic features (*7*). Fourth, the number of methyl groups bound per enzyme (0.5 methyl group per $\alpha\beta$) suggests that only Ni-labile A-clusters can be methylated (*15*). Fifth, Mössbauer results suggest that only about 40% of C_{ox} clusters reduce to C_{red1} and eventually to C_{red2} (*14*). The remaining clusters are reduced by one electron to an $S = {}^3/_2$ state called $C_{3/2}$. This reduction corresponds to the process $[Fe_4S_4]^{2+} + e^- = [Fe_4S_4]^{1+}$. Sixth, only about 70% of B-clusters can be reduced to the B_{red} $S = {}^1/_2$ state, affording the $g_{av} = 1.94$ signal (*9*, *10*). The remaining B_{red} $[Fe_4S_4]^{1+}$ clusters are tentatively thought to have an S of ${}^3/_2$, because the enzyme exhibits EPR features (g) between 4 and 6 (*14*).

The origin of this heterogeneity is not understood. Obvious possibilities, such as impurities, damage during protein purification, and errors in protein, spin, and/or metal analyses, have been considered and discounted (*19*). Lacking a coherent explanation of this phenomenon, we decided to ascertain whether the low-intensity EPR signals arise because only a fraction of the redox centers in the enzyme are reduced to the observed EPR-active states, or because of a physical effect attenuating EPR intensity (*20*). We also wanted to determine whether ACS contains other redox centers besides A−C. Our approach was to titrate oxidized ACS with the reductant CO, monitor samples by EPR, and simulate the resulting titration curves assuming various models that explain the heterogeneity. This method can detect spectroscopically unobservable redox sites, and has been successfully applied to the NiFe hydrogenase from *Desulfovibrio gigas* (*21*, *22*).

In this paper, we report the results and analysis of our titrations. We conclude that the intensities of ACS EPR signals are low because the enzyme suffers from the redox and spin-state heterogeneity previously proposed, and that within the potential region reliably probed by these titrations, there are no additional EPR-silent species in the enzyme.

EXPERIMENTAL PROCEDURES

Isolation of ACS. C. thermoaceticum cells were grown, and three batches of ACS were purified as described previously (*19*). Purification, preparation of samples, and titrations were performed in an Ar atmosphere glovebox (Vacuum/Atmospheres, HE-453) containing <1 ppm O_2 as detected continuously by a calibrated Teledyne model 310 analyzer. All buffers were degassed on a Schlenk line, transferred into the glovebox, and exposed to the glovebox atmosphere overnight to remove residual O_2. Research grade CO and CO_2 were O_2-scrubbed (Oxisorb, MG Scientific) prior to use. Batches 1−3 had CO oxidation activities of 340, 240, and 320 units/mg, and CO−acetyl-CoA exchange activities of 0.21, 0.18, and 0.26 units/mg, respectively (*23*, *24*). All batches were >90% pure as determined by visual inspection of SDS−polyacrylamide electrophoretic gels. Protein concentrations were determined by the Biuret method (*25*).

Titrations with CO. Three CO titrations (1−3) of ACS under a CO_2 atmosphere (CO/CO_2) were performed, using batches 1−3, respectively. Modified EPR cuvettes with quartz mixing chips and intentionally punctured rubber septa (*4*) were prepared. ACS was concentrated (30 000 MW Centricon concentrator) and passed down a 1.5 cm × 15 cm Sephadex G-25 column equilibrated in 50 mM MES (pH

[2] The atmosphere and pH are relevant because the presence of CO_2 shifts the redox potential and CO binding properties of the enzyme (*8*). Unless mentioned otherwise, all potentials quoted here were obtained for ACS under CO_2 at pH 6.3, and are relative to the normal hydrogen electrode.

6.3). The eluent (17.5 mg/mL of ACS for titration 2) was diluted to 4.0 mg/mL with elution buffer, incubated in a CO_2-filled vial for 45 min, and then used to completely fill the EPR cuvettes (leaving no gas phase). Had a gas phase been present, added CO would have partitioned into it, complicating calculations. Cuvettes were injected with increasing volumes of either CO-saturated buffer at 26 °C [970 μM CO (*26*)] or 1.00 mM thionin [standardized against potassium ferricyanide as described previously (*13*)]. Cuvette solutions were mixed by repeated inversion for 1 min, incubated for an additional 1 min, and then frozen by rapid immersion in liquid N_2-cooled isopentane. ACS was titrated similarly with CO under an Ar atmosphere (CO/Ar) except that the enzyme (26 μM, batch 3) was incubated under Ar prior to filling EPR cuvettes and the concentration of the thionin solution was 0.86 mM.

Analysis. EPR spectra were recorded as described previously (*4*). Spectra consisted of some combination of the NiFeC and $g_{av} = 1.94$, 1.82, and 1.86 signals. Individual signals were simulated using the XPOW program (*27*−*30*). Simulated signals were double-integrated and quantified using a 1.00 mM Cu perchlorate standard (*31*). Resulting spin concentrations (normalized per ACS $\alpha\beta$) were plotted versus the number of equivalents of CO added (also normalized per $\alpha\beta$). Such plots will be called the A_{red}−CO, B_{red}, C_{red1}, and C_{red2} titration curves. After EPR analysis, concentrations of Ni and Fe were determined by electrothermal ionization atomic absorption spectrometry (Perkin-Elmer model 2380). Prior to analysis, samples were digested overnight at 80 °C in 6 M trace-metal grade nitric acid. Samples from titrations 1 and 3 were also subjected to quantitative amino acid analysis, using the methods of Moore and Stein (*32*) for titration 1 and those of Godel et al. (*33*) for titration 3. The enzyme concentrations (E_{tot}) used in the analyses were the average of the Biuret, amino acid analysis, the Ni concentration divided by 2, and the Fe concentration divided by 12. For titration 1, the respective values (in micromolar) were 28, 28, 27, and 26, yielding an E_{tot} of 27 μM. For titration 3, the respective values were 26, 20, 31, and 23, yielding an E_{tot} of 25 μM. For titration 2, the Biuret, Ni, and Fe values were 26, 26, and 24, respectively, yielding an E_{tot} of 25 μM. We estimate an overall relative uncertainty in E_{tot} of ±15%.

Simulations. Each simulated titration curve consisted of 100 individual "simulation points" evenly spaced at intervals spanning the range (in either equivalents per $\alpha\beta$ or in atmospheres) of the experimental titrations. At each point, the specified amount of CO was presumed to reduce the A-, B-, and C-clusters and an unidentified EPR-silent $n = 2$ redox site (called X) according to expressions 3−8 at fixed pH.

$$2R_A[A_{ox}] + 3R_A[CO] \rightleftharpoons 2R_A[A_{red}{-}CO] + R_A[CO_2] \quad (3)$$

$$2R_B[B_{ox}] + R_B[CO] \rightleftharpoons 2R_B[B_{red}] + R_B[CO_2] \quad (4)$$

$$2R_C[C_{ox}] + R_C[CO] \rightleftharpoons 2R_C[C_{red1}] + R_C[CO_2] \quad (5)$$

$$2R_C[C_{red1}] + R_C[CO] \rightleftharpoons 2R_C[C_{int}] + R_C[CO_2] \quad (6)$$

$$2R_C[C_{int}] + R_C[CO] \rightleftharpoons 2R_C[C_{red2}] + R_C[CO_2] \quad (7)$$

$$R_X[X_{ox}] + R_X[CO] \rightleftharpoons R_X[X_{red}] + R_X[CO_2] \quad (8)$$

where R_N (N being A, B, C, or X) values indicate the proportion of redox site N presumed to be redox-active. For each simulation point, $[N_J]$ values are the equilibrium concentrations of center N in a given state J (J being ox, red, or red-CO) divided by E_{tot}.

Equilibrium constants for reactions 3−8 were calculated from the equation $K_{eq} = \exp(nF/RT)\Delta E°$, where $\Delta E° = (E°_{ox/red} - E°_{CO_2/CO})$. $E°_{CO_2/CO}$ is the thermodynamic reduction potential for the CO_2/CO couple, −0.487 V at pH 6.3 (*34*). $E°_{ox/red} = -0.173$ V for A_{ox}/A_{red}−CO in reaction 3 (*5*), −0.366 V for B_{ox}/B_{red} in reaction 4 (*8*), −0.345 V for C_{red1}/C_{int} and C_{int}/C_{red2} in reactions 6 and 7, respectively (*8*), and unknown for C_{ox}/C_{red1} in reaction 5 and X_{ox}/X_{red} in reaction 8. $E°_{ox/red}$ values were determined using partial pressures for CO and CO_2. P_{CO} and P_{CO_2} are the partial pressures of CO and CO_2, respectively. P_{CO_2} was fixed at 1 atm for all points. The CO concentration for each sample was known from the amount of CO-saturated buffer injected, but the P_{CO} values used in solving the equilibrium expressions had to be calculated using Henry's Law since there was no gas phase.

Values of R_N were model-dependent, and are specified in Table 1 and the Supporting Information. Equilibrium expressions for reactions 3−8 were determined at each simulation point using the following iterative procedure. Reaction 3 was allowed to equilibrate, using the initial P_{CO} for that simulation point. The amount of CO remaining was used as the initial pressure to solve reaction 4. The equilibrium P_{CO} obtained from reaction 4 was used as the initial P_{CO} for reaction 5, etc. until the equilibrium P_{CO} for reaction 8 was obtained. This cycle was repeated a sufficient number of times (determined experimentally to be 30) for all reactions to be simultaneously at equilibrium. The fact that this condition was achieved was determined by verifying that all equilibrium constants calculated using the final concentrations and pressures equaled the values generated from the supplied $E°_{ox/red}$ values.

Equilibrium concentrations were related to spin concentrations (spins per $\alpha\beta$) of the NiFeC and $g_{av} = 1.94$, 1.82, and 1.86 EPR signals (designated I_{NiFeC}, $I_{1.94}$, $I_{1.82}$, and $I_{1.86}$, respectively) through eqs 9−12.

$$I_{NiFeC} = S_A R_A [A_{red}{-}CO]/E_{tot} \quad (9)$$

$$I_{1.94} = S_B R_B [B_{red}]/E_{tot} \quad (10)$$

$$I_{1.82} = S_C R_C [C_{red1}]/E_{tot} \quad (11)$$

$$I_{1.86} = S_C R_C [C_{red2}]/E_{tot} \quad (12)$$

where S_N (N being A, B, or C) is the proportion of the designated redox-active cluster that contributes to the associated EPR signal intensity.

Simulated EPR intensity titration curves were compared to the experimental curves as described below. All points shown in the figures were included in this process. The resulting quality-of-fit parameter Q_{fit} is essentially the average normalized length between each data point and the nearest simulation point; thus, smaller Q_{fit} values correspond to better fits. To minimize Q_{fit}, $E°_{C_{ox}/C_{red1}}$ and $E°_{X_{ox}/X_{red}}$ were freely adjusted, and S_A, S_B, S_C, R_A, R_B, R_C, and R_X values were allowed to vary within 15% of their model-requiring values given in Tables 2−5. $E°_{A_{ox}/A_{red}}$, $E°_{B_{ox}/B_{red}}$, $E°_{C_{red1}/C_{int}}$, and $E°_{C_{int}/C_{red2}}$ were fixed at the experimentally determined values

given above. Within these constraints, Q_{fit} values were normalized to the best (lowest) Q_{fit} obtained (called Q_{bfit}).

Models Employed. The partial-plus-X (or PPX) model assumes the redox chemistry attributed to the A-, B-, and C-clusters in the introductory section and the presence of another (generic) redox site X. The word "partial" indicates the assumption of redox heterogeneity. If the PPX model were correct, the number of electron equivalents per $\alpha\beta$ accepted by fully oxidized ACS would depend on the EPR spin intensities. As an example, assume I_{NiFeC}, $I_{1.94}$, $I_{1.82}$, and $I_{1.86}$ values of 0.20, 0.75, and 0.4 spin/$\alpha\beta$, respectively. According to a recent Mössbauer study, an I_{NiFeC} of 0.2 spin/$\alpha\beta$ would indicate 0.3 redox-active $A_{red}-CO$ center/$\alpha\beta$ ($R_A = 0.3$ and $S_A = 0.7$) (*7*). Each cluster in the A_{ox} state requires 3 equiv/$\alpha\beta$ for reduction to $A_{red}-CO$, yielding a subtotal of 0.9 equiv/$\alpha\beta$ involved in reducing the A-cluster. All B-clusters are assumed to be redox-active ($R_B = 1.0$) and require 1 electron for reduction (subtotal of 1.0 equiv/$\alpha\beta$ involved in reducing the B-cluster). About 75% of B-clusters are assumed to reduce to the $S = {}^1/_2$ B_{red} state, yielding the $g_{av} = 1.94$ signal with a maximal intensity $I_{1.94}$ of 0.75 spin/$\alpha\beta$ (thus, $S_B = 0.75$), while 25% reduce to the $S = {}^3/_2$ B_{red} state, yielding EPR features (g) between 4 and 6. About 40% of C-clusters are assumed to reduce from C_{ox} to C_{red2} (a three-electron process, with an I_C of 0.4 spin/$\alpha\beta$ and an S_C of 1.0), and the remainder are reduced by one electron to the $C_{S=3/2}$ state. This yields a subtotal of $(3 \times 0.4) + 0.6$ (=1.8) equiv/$\alpha\beta$ used to reduce both forms of the C-cluster. We do not know the redox potential of the $C_{ox}/C_{S=3/2}$ couple, but assume that of the B_{ox}/B_{red} couple (both reductions correspond to the one-electron reduction of an $[Fe_4S_4]^{2+}$ cube). For simplicity, we count the proportion of C-clusters that reduce to the $C_{S=3/2}$ state along with the B-clusters, affording an R_B of $1.0 + 0.6$ (=1.6) redox-active clusters/$\alpha\beta$ and an S_B of 0.75/1.6 (=0.47). That leaves an R_C of 0.4 and an S_C of 1.0, where these values refer only to those C-clusters that can be reduced to the C_{red1} and C_{red2} states. In the PPX model, the proportion of site X (R_X) is variable. In general, the PPX model predicts that the number of equivalents per $\alpha\beta$ accepted by fully oxidized ACS equals

$$EQ_{tot}\ (\text{equiv}/\alpha\beta) = 3R_A[A_{tot}] + 1R_B[B_{tot}] + 3R_C[C_{tot}] + 1(1 - R_C)[C_{tot}] + 2R_X[X_{tot}] \quad (13)$$

The five terms in eq 13 indicate the number of equivalents per $\alpha\beta$ accepted by the A, B, and C (those that reduce to the C_{red1} and C_{red2} states), C (those that reduce to the $C_{S=3/2}$ state), and X redox sites, respectively. In the example presented above, if site X accepted 0.6 equiv/$\alpha\beta$ ($R_X = 0.3$), EQ_{tot} would equal $(3 \times 0.3 \times 1) + (1 \times 1.0 \times 1) + (3 \times 0.4 \times 1) + (1 \times 0.6 \times 1) + (2 \times 0.3 \times 1)$, or 4.3 equiv/$\alpha\beta$.

The partial-minus-X (or PMX) model is identical to the PPX model except that it excludes the X site. Given the maximum EPR signal intensities and the PMX model, EQ_{tot} can be obtained from eq 14.

$$EQ_{tot}\ (\text{equiv}/\alpha\beta) = 3I_{NiFeC}[A_{tot}]/S_A + I_{1.94}[B_{tot}]/S_B + 3[(I_{1.82} + I_{1.86})/2][C_{tot}]/S_C + 1[1 - (I_{1.82} + I_{1.86})/2][C_{tot}]/S_C \quad (14)$$

In this example, $EQ_{tot} = (3 \times 0.2)/0.7 + (1 \times 0.75)/0.75 + (3 \times 0.4)/1 + (1 \times 0.6)/1$, or 3.7 equiv/$\alpha\beta$.

The total-plus-X (or TPX) model is identical to the PPX model except that it assumes that all clusters in the enzyme are redox-active (thus, no redox heterogeneity in the enzyme) whether they exhibit EPR signals (i.e., $R_A = R_B = R_C = R_X = 1.0$, and $S_A = I_A$, $S_B = I_B$, and $S_C = I_C$). The TPX model predicts that fully oxidized ACS would accept 9 equiv/$\alpha\beta$ in the CO/CO_2 titration. The total-minus-X (or TMX) model is identical to the TPX model except that it excludes the X site; it predicts that fully oxidized ACS would accept 7 equiv/$\alpha\beta$.

The entire experiment and analysis employs 22 parameters, including (a) the protein concentration; (b) the initial CO concentration at each point; (c) the CO_2 concentration; (d) the pH; (e) the observed spin intensities for the NiFeC and $g_{av} = 1.94$, 1.82, and 1.86 signals; (f) the redox potentials for the $A_{ox}/A_{red}-CO$, B_{ox}/B_{red}, C_{ox}/C_{red1}, C_{red1}/C_{int}, C_{int}/C_{red2}, and X_{ox}/X_{red} couples; (g) the proportion of each center that is redox-active (R_A, R_B, R_C, and R_X); (h) the proportion of each redox-active center that exhibits an EPR signal (S_A, S_B, and S_C); and (i) the number of equivalents per $\alpha\beta$ by which the enzyme is reduced at the start of the titration (EQ_{init}). This last parameter is required because the samples were not fully oxidized at the start of the titrations (see below for more details).

RESULTS

Three independent reductant-free samples of ACS were titrated under a CO_2 atmosphere using stoichiometric amounts of the reductant CO and the oxidant thionin, as described in Experimental Procedures. The extent of reaction was monitored by EPR. Resulting spectra were simulated, and the intensities of each contributing signal were quantified and plotted as titration curves. These curves were simulated using parameters defined by particular models.

Selected 10 K spectra from one titration (Titration 2) are shown in Figure 1. The most oxidized sample (Figure 1A) exhibited only the $g_{av} = 1.82$ signal (from the C_{red1} state). As CO was added and samples were incrementally reduced, this signal increased, and then declined as the $g_{av} = 1.86$ (from C_{red2}), 1.94 (from B_{red}), and NiFeC (from $A_{red}-CO$) signals arose and eventually plateaued. Intensities of the $g_{av} = 1.82$ and 1.86 signals were obtained from the 20 mW spectra (Figure 1, upper set of spectra). NiFeC and $g_{av} = 1.94$ signal intensities were quantified from the 0.05 mW spectra (Figure 1, lower set of spectra), since they saturated at 20 mW. For each titration, with increasing amounts of CO, the intensity of the C_{red1} state increased to a maximum, and then declined as the intensity of C_{red2} increased and eventually plateaued. The most distinctive points of these curves are the initial increase in the C_{red1} intensity, the "hump" in the C_{red1} intensity, and the C_{red1}:C_{red2} "crossover point". Each titration began at a slightly different oxidation state, and so for ease of viewing (Figures 2−4), titrations were aligned at the C_{red1}:C_{red2} crossover points (where all three samples share a common oxidation state).

Before describing the analysis of these data, we must mention difficulties encountered and our methods of resolving them. This is important because the degree to which we succeeded in resolving these difficulties impacts our conclusions.

"Spontaneous" Oxidation of Fully Reduced ACS. Titrations were complicated by spontaneous reactions apparently

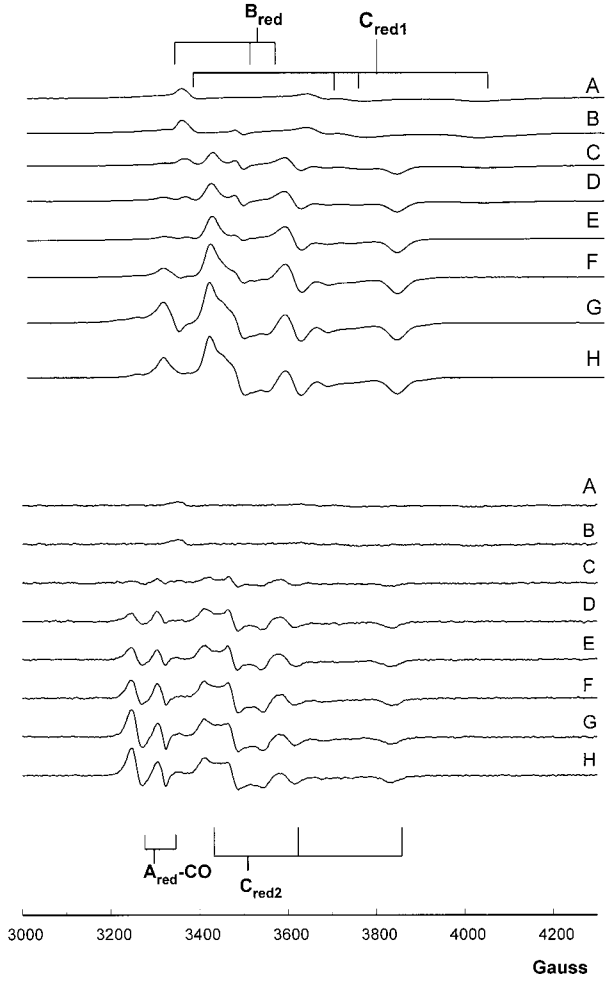

FIGURE 1: Selected EPR spectra of CO/CO_2 titration 2 collected at microwave powers of 20 (top panel) and 0.05 mW (bottom panel). Samples were treated with the following amounts (equivalents per $\alpha\beta$) of either CO or thionin: (A) 0.375, thionin; (B) 0.0; (C) 0.75, CO; (D) 1.25, CO; (E) 1.5, CO; (F) 2.0, CO; (G) 4.0, CO; and (H) 6.0, CO. Data points were subsequently readjusted to the ideal starting point of the titration as described in Experimental Procedures. EPR conditions were as follows: microwave frequency, 9.42 GHz; temperature, 10 K; modulation amplitude, 11.8 G; and modulation frequency, 100 kHz. CO equivalents (and thionin equivalents) are equal to electron equivalents.

catalyzed by ACS. Fully reduced enzyme spontaneously oxidizes apparently because of a slow hydrogenase activity (*35*, *36*). At equilibrium, the enzyme is in a stable partially reduced state. Despite this, we wanted to generate complete titration curves (from fully oxidized to fully reduced). Because of its stability, the partially reduced state (most conveniently obtained by removing all reductants chromatographically) was chosen as the titration start point. To generate the complete titration, some aliquots had to be oxidized while others were reduced, and all were subsequently frozen before they equilibrated back to the partially reduced state. This approach effectively achieved equilibrium conditions for catalytically functional redox processes occurring in the reductive part of the titrations. It was effective because the rates of reduction of catalytically functional redox sites are fast relative to the hydrogenase activity (*23*, *36*).

Spontaneous Reduction of Fully Oxidized ACS. Fully oxidized ACS (oxidized with excess thionin) spontaneously reduces to a partially reduced state, apparently because excess

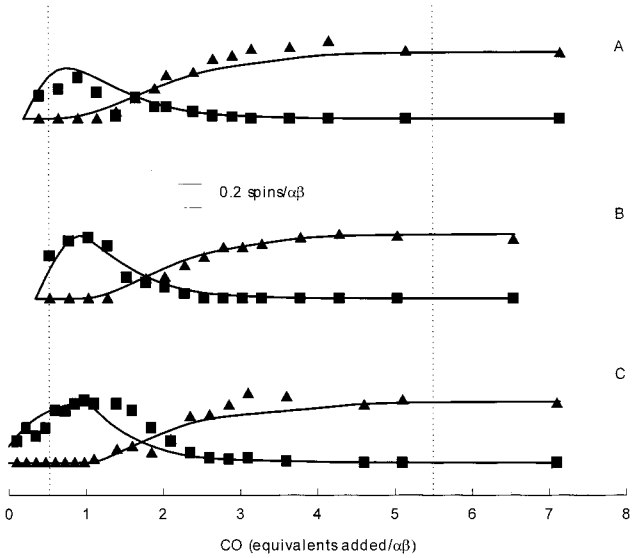

FIGURE 2: C-Cluster curves for titrations 1 (A), 2 (B), and 3 (C): (■) C_{red1} and (▲) C_{red2}. Solid lines are the best fits using the PPX model. For clarity, curves A and B have been shifted vertically by 0.7 and 1.4 spins/$\alpha\beta$, respectively. Other details are given in the text and Table 1.

thionin oxidatively damages the metal clusters in ACS, releasing sulfide ions that reduce other enzyme molecules (*35*). This problem was less easily resolved. Milder oxidants could not be used because they would not oxidize the enzyme fully, and excess thionin irreversibly inactivates the enzyme at a rate that becomes (at thionin amounts of greater than $\sim$1 equiv/$\alpha\beta$) comparable to that at which catalytically functional oxidation processes occur (*35*). As a result, fully active and fully oxidized ACS (i.e., devoid of the C_{red1} EPR signal) could not be obtained.

C_{red1} and C_{red2} Titration Curves. The C_{red1} curves for the three titrations are shown in Figure 2. For titrations 1 and 2, the most oxidized regions (where 1.0−3.0 equiv/$\alpha\beta$ of thionin was added) are not presented. In those regions, the intensity of C_{red1} declined far slower with added thionin than expected if the only oxidation process occurring was $C_{red1} \rightarrow C_{ox}$. We took this as evidence for the inactivation oxidation processes described above, and excluded these points. This problem was not as apparent for titration 3, and so all points were included.

Thus, the most oxidized samples included in the titration curves were not fully oxidized at the start point of the titrations; all of the A- and B-clusters were oxidized, but a fraction of the C-clusters were in the C_{red1} state (with the remainder in the C_{ox} state). It was important for our analysis to determine the point at which the titrations would have begun had those inactivation oxidation processes been absent (the "ideal" start point). The ideal start point was estimated by simulating the shape of the reliable portion of the C_{red1} hump region (assuming just the $C_{ox} \rightarrow C_{red1}$ redox process) and "constructing" the most oxidized portion of the C_{red1} titration curve. This resulted in the curve that would have been present had the inactivation oxidation processes been absent. The experimental titration curves were then shifted by a variable amount designated EQ_{init} to minimize Q_{fit}. EQ_{init} is defined as the number of equivalents per $\alpha\beta$ between the first reliable experimental data point and the ideal start point of the titrations. This procedure was also performed on titration 3, even though no data points had been excluded.

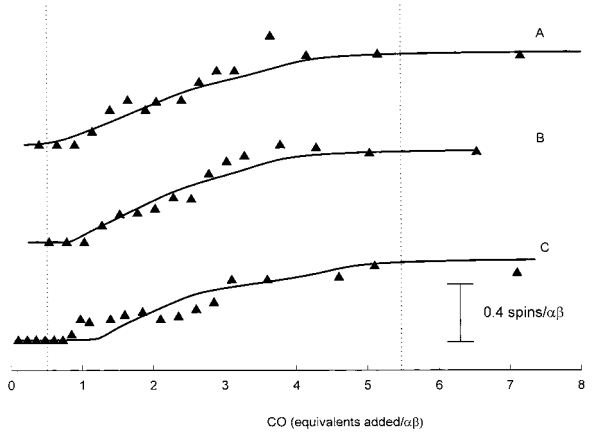

FIGURE 3: B-Cluster titration curves. Details as described in the legend of Figure 2.

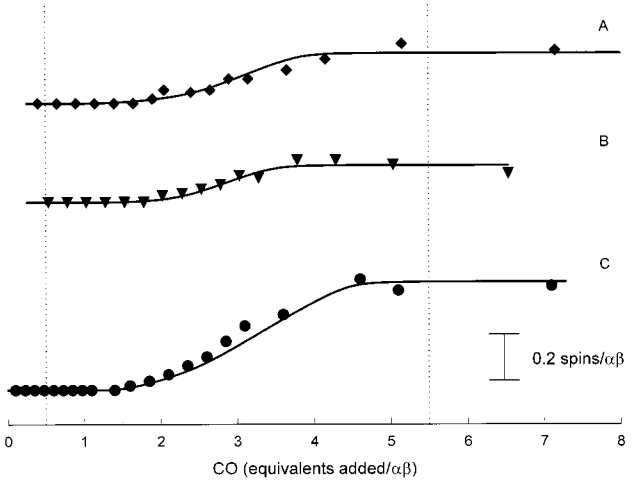

FIGURE 4: A-Cluster titration curves. Details as described in the legend of Figure 2.

Despite complexities, uncertainties resulting from this procedure were not large. The first reliable data points in the C_{red1} titration curves were located on the oxidative decline of the C_{red1} hump region (to the right of the left dotted vertical line in Figure 2), and so the curvature of that region could be used to extrapolate to the abscissa (at 0 spin/$\alpha\beta$). Moreover, the C_{red1} spin intensities of the first reliable points were no greater than 0.2 spin/$\alpha\beta$, and so only 0.2 equiv/$\alpha\beta$ (assuming the partial models) or 0.5 equiv/$\alpha\beta$ (assuming the total models) of oxidizing equivalents would be required to abolish that signal. Thus, the uncertainty in this procedure corresponded to less than ~10% of the total number of titrated equivalents. It did, however, add uncertainty to the determination of $E°_{C_{ox}/C_{red1}}$ and the presence of high-potential EPR-silent redox sites (see below).

The average of the best-fit values for $E°_{C_{ox}/C_{red1}}$ (−0.12 V) should be reliable within 40 mV. This value, along with $E°_{C_{red1}/C_{int}}$, determines the shape of the C_{red1} hump. Given that there was no inactivation oxidation occurring in the bulk of this hump region, the fit to it should be fairly accurate. An $E°_{C_{ox}/C_{red1}}$ of −0.22 V has been reported for samples under Ar (*9*), suggesting a CO_2-dependent shift of 0.1 V. This is in line with the effects of CO_2 on other redox processes in the enzyme.

The C_{red2} titration curves were quite reproducible for the three titrations, while the C_{red1} titration curves, and in particular the intensity of the C_{red1} humps, varied significantly. In titration 1, the maximum intensity of this feature was only 50% of the maximal intensity of the C_{red2} state, while in the other two titrations, the C_{red1} and C_{red2} maximal intensities essentially matched. We have observed similar variations in previous studies, but typically, the C_{red1} and C_{red2} maximal intensities have been quite similar (*8*, *9*, *13*). Thus, we regard the attenuated intensity of the C_{red1} curve of titration 1 as anomalous.

B_{red} and A_{red}−CO Titration Curves. The B_{red} titration curves, shown in Figure 3, were quite reproducible. In each case, essentially all ACS molecules of the most oxidized samples contained B_{ox}. The B_{red} state began to develop at ~1 equiv/$\alpha\beta$; its intensity increased monotonically to 4.5 equiv/$\alpha\beta$, and plateaued thereafter.

The A_{red}−CO titration curves are shown in Figure 4. All ACS molecules in the most oxidized samples contained A_{ox}. The A_{red}−CO state began to develop between 1.5 and 1.8 equiv/$\alpha\beta$; its intensity increased monotonically, and plateaued at 3.5−4.5 equiv/$\alpha\beta$. As observed in numerous previous studies, the NiFeC signal intensities varied substantially for the three titrations (*8*, *9*, *13*, *15*).

Simulation of Titration Curves. Titration curves were simulated using four model descriptions of the redox properties in ACS. The simulation procedures and the PPX, PMX, TPX, and TMX models are described fully in Experimental Procedures. Numerous parameters were required for these simulations, but many were known from previous studies and were not varied. Others (defined by the model that was employed) were allowed to vary slightly. *The most remarkable aspect of this study is that, despite these severe restrictions, the simulations to the partial models (PPX and PMX) fit the data extremely well.* Best-fit parameters are given in Table 1, and simulations are shown in Figures 2−4 (solid lines). Neither total model (TPX and TMX) fit the data satisfactorily (see Tables A and B of the Supporting Information), yielding Q_{fit} values 1.6−5.8 times Q_{bfit}. This result indicates that the total models are incorrect.

According to eq 14 and the values in Table 1, the best-fit total number of reducing equivalents per $\alpha\beta$ accepted by the samples was 3.5 for titration 1 (PMX model), 3.7 for titration 2 (PPX model), and 5.0 for titration 3 (PPX model). Titration 3 accepted more equivalents than titrations 1 and 2 primarily because I_{NiFeC} was substantially higher in titration 3, and this increased R_A. Titration 2 accepted more equivalents than titration 1 primarily because the $g_{av} = 1.82$ signal intensity was disproportionately low in titration 1.

Titrations of ACS with CO under an Ar Atmosphere. ACS titrations with CO performed under Ar are more complicated to analyze, since the Nernst equation cannot be reliably employed. The problem is that the concentration of CO_2 is very low in these titrations and can only be estimated (*8*). Nevertheless, the differences in the pattern of signal development are edifying, and so we present selected EPR spectra of a CO/Ar titration in Figure 5. The corresponding titration curves are shown in Figure 6. The sample devoid of CO was partially reduced with 0.05 spin/$\alpha\beta$ for B_{red} and 0.14 spin/$\alpha\beta$ for C_{red1}. The intensity of the B_{red} state increased rapidly (with a slope of 0.4 spin/equiv) and was fully developed by 1 equiv/$\alpha\beta$. The C_{red1}:C_{red2} conversion began at 0.5 equiv/$\alpha\beta$, had a crossover point at 1.2 equiv/$\alpha\beta$, and was complete at ~2.5 equiv/$\alpha\beta$. The A_{red}−CO state began

Table 1: Theoretical and Best-Fit Parameters Using the PPX and PMX Models

	titration 1 (PPX)	titration 1 (PMX)	titration 2 (PPX)	titration 2 (PMX)	titration 3 (PPX)	titration 3 (PMX)
S_A	0.65 (0.70)[a]	0.65 (0.70)	0.66 (0.70)	0.70 (0.70)	0.81 (0.70)	0.78 (0.70)
S_B	0.46 (0.41)	0.46 (0.41)	0.46 (0.41)	0.44 (0.41)	0.31 (0.31)	0.30 (0.31)
S_C	1.15 (1.00)	1.15 (1.00)	1.15 (1.00)	1.00 (1.00)	1.00 (1.00)	1.00 (1.00)
R_A	0.35 (0.30)	0.33 (0.30)	0.26 (0.30)	0.27 (0.30)	0.55 (0.60)	0.55 (0.60)
R_B	1.50 (1.60)	1.40 (1.60)	1.50 (1.60)	1.60 (1.60)	1.60 (1.60)	1.80 (1.60)
R_C	0.36 (0.40)	0.38 (0.40)	0.34 (0.40)	0.40 (0.40)	0.35 (0.40)	0.40 (0.40)
R_X	0.25 (0.30)	−	0.26 (0.30)	−	0.44 (0.5)	−
EQ_{int}	0.10	0.20	0.25	0.20	0.20	0.20
$E°_{C_{ox}/C_{red1}}$	−0.100	−0.100	−0.15	−0.15	−0.20	−0.20
$E°_{X_{ox}/X_{red}}$[b]	−0.20	−	−0.15	−	−0.20	−
Q_{bfit}	1.08	1.00	1.00	1.13	1.00	1.16

[a] Theoretical values are shown in parentheses. [b] For all models, $E°_{A_{ox}/A_{red}-CO} = -0.173$ V, $E°_{B_{ox}/B_{red}} = -0.366$ V, and $E°_{C_{red1}/C_{int}} = E°_{C_{int}/C_{red2}} = E°_{C_{red1}/C_{red2}} = -0.345$ V.

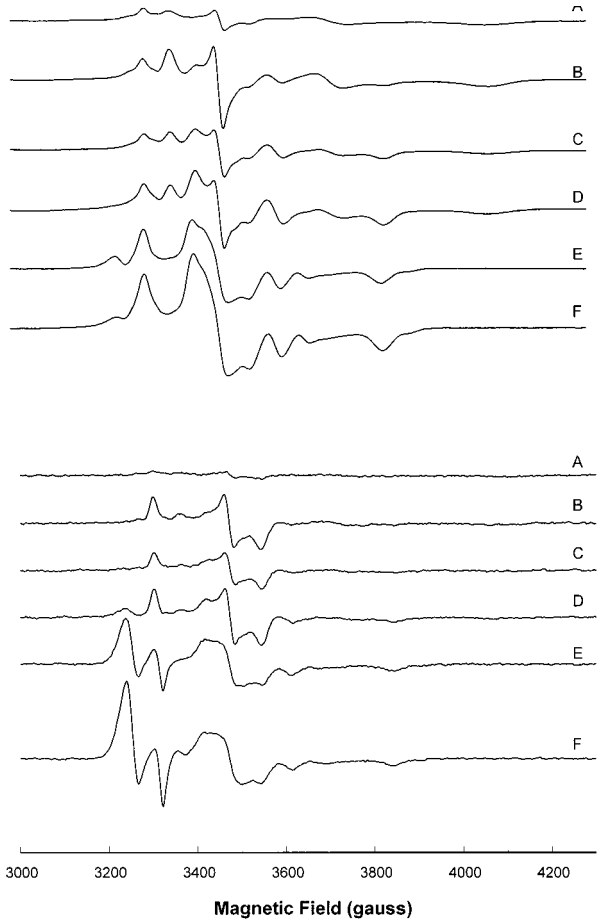

FIGURE 5: Selected EPR spectra from the titration of ACS with CO under Ar. EPR conditions as described in the legend of Figure 1. The amounts of CO added, in equivalents per $\alpha\beta$, were (A) 0.0, (B) 0.5, (C) 1.0, (D) 1.5, (E) 3.0. and (F) 5.0.

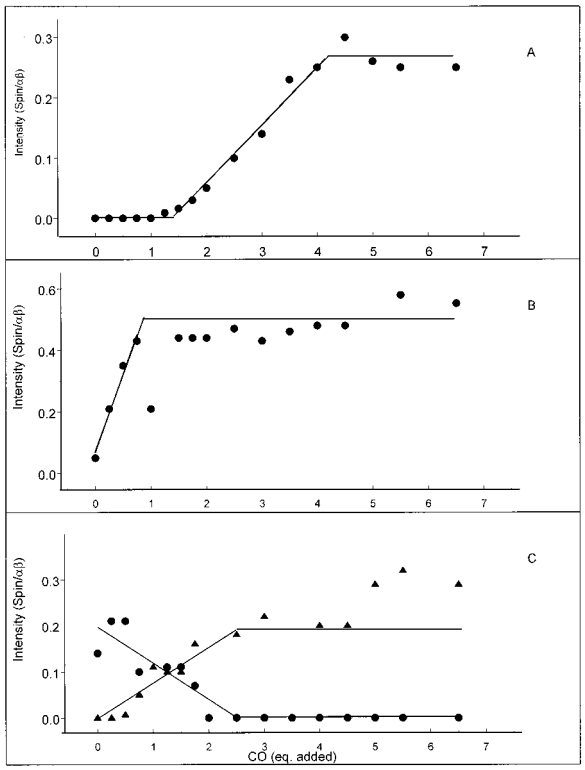

FIGURE 6: Titration curves for CO/Ar: (A) A_{red}−CO (NiFeC EPR signal intensity vs the number of equivalents per $\alpha\beta$ of CO), (B) B_{red} ($g_{av} = 1.94$ signal), and (C) C_{red1} [$g_{av} = 1.82$ (●)] and C_{red2} [$g_{av} = 1.86$ (▲)] titration curves. Solid lines were constructed by visual inspection of the data.

to develop at 1.5 equiv/$\alpha\beta$ and was complete at ∼4 equiv/$\alpha\beta$.

Is an Additional EPR-Silent Redox Site X Present in ACS? An important issue is whether these titrations support the presence of an EPR-silent redox site in ACS. The best-fit simulation to titration 1 (PMD) assumed no X site in ACS, while those to titrations 2 and 3 assumed 0.5 and 0.9 equiv/$\alpha\beta$ for X, respectively. Thus, these data are unable to rigorously support or exclude the existence of X. However, closer inspection of the data reveals that the best-fit $E°_{X_{ox}/X_{red}}$ for both titrations essentially matches $E°_{C_{ox}/C_{red1}}$ (−0.15 and −0.20 V for titrations 2 and 3, respectively). Thus, the fitting program "used" X to fit the region of the titrations where the C_{ox}/C_{red1} couple is active, i.e., the oxidative side of the C_{red1} hump. This was the most difficult region to analyze because another oxidative process occurred there. Even if the fitting procedure was prompted with $E°_{X_{ox}/X_{red}}$ values substantially more negative than $E°_{C_{ox}/C_{red1}}$, the iterative nature of the program eventually shifted the former value toward the latter. For titrations 1 and 2, data beyond the last reliable point in Figures 2−4 were excluded, while for titration 3, all data that were collected were included. In retrospect, some oxidative inactivation probably accounted for the broad decline in the oxidative side of the hump in titration 3, and this was attributed to site X. Thus, the site X used to improve the fit in titrations 2 and 3 is almost certainly not the functional redox site X or D proposed previously (*13*, *15*−*17*).

DISCUSSION

Heterogeneity of ACS. The excellent fits of the partial models to the titration data, using very few free-floating parameters, provide strong evidence that ACS is heterogeneous as previously proposed (*6*, *7*, *9*, *10*, *14*, *15*, *18*, *19*) and described in the introductory section. The origin of this heterogeneity remains unknown, though (a) harvesting *C. thermoacetica* anaerobically, (b) purifying ACS under strict anaerobic conditions, (c) purifying ACS rapidly in the presence of DTT, and (d) purifying ACS without excessive prolonged dilution all seem to yield somewhat higher activities and spin intensities (*15*). However, even when purified under these conditions, the greatest NiFeC and $g_{av} = 1.82$ or 1.86 signal intensities correspond to ~0.5 and ~0.4 spin/αβ, respectively (i.e., similar to titration 3). Heterogeneity may ultimately arise from events occurring during the growth of the bacteria. Similar heterogeneity seems to afflict a number of other proteins besides ACS, including methane monooxygenase (*37*, *38*), ribonucleotide reductase (*39*), and stearoyl-acyl carrier protein Δ-9 desaturase (*40*).

EPR-Silent Redox Sites. Our data and analysis indicate that there are no additional EPR-silent redox sites titrating in the region between 0.3 and 6 equiv/αβ. If such a site is assumed, the fitting process "shifts" the potential so that the assumed site undergoes redox in the most oxidative portion of the titrations (from 0 to 0.3 equiv/αβ). In fact, the "site" fitted by our models is probably due to oxidative inactivation that occurs upon adding thionin. There may also be EPR-silent species (e.g., the D site) that titrate beyond the end point of our titration (where all of the EPR signals cease changing), but these would be undetected. $E°$ for such a species would likely be less than −0.45 V. Under an Ar atmosphere, the reduction potential of the D site is about −0.54 V. In the presence of CO_2, this potential may be less negative, but given the function of the D site (to render the Ni^{2+} of A_{ox} a potent nucleophile), its potential under CO_2 should remain quite negative, beyond the range of the titrations that are presented.

Comparison to Previous Titrations. Lindahl et al. (*9*) first titrated ACS, using the method of controlled potential coulometry. In the potential region between −0.1 and −0.6 V, 5.4 equiv/αβ of electrons was accepted by the thionin-oxidized enzyme under an Ar atmosphere. These electrons reduced B_{ox} to B_{red} and C_{ox} to C_{red1} and converted C_{red1} to C_{red2}. The partial model predicts that oxidized ACS would require ~1 equiv/αβ less in Ar than in CO_2 (since the A-cluster would not be reduced). Thus, the samples used by Lindahl et al. (*9*) accepted about 2 equiv/αβ more than that predicted by the PPX model (assuming standard spin intensities). At the time of the previous study, the deleterious effects of thionin were not known, and we suspect that oxidative inactivation products consumed the extra reducing equivalents.

Shin et al. (*35*) performed both oxidative and reductive stoichiometric titrations, using CO as a reductant and thionin as an oxidant, monitoring the reaction by UV−vis spectroscopy. They found that ACS contained "A_{420}-sensitive" redox sites that could accept or donate ~4 equiv/αβ and were most likely involved in catalysis. Their results are compatible with those obtained here.

Seravalli et al. (*16*) reported stoichiometric reductive titrations of ACS with dithionite and CO, monitored with EPR and UV−vis. Their samples began partially reduced, with C_{red1} and B_{red} EPR signals each quantifying to about 0.2 spin/αβ. According to the PMX model, these samples would have been about 0.4 equiv/αβ reduced. With dithionite as the reductant, the titration was complete after adding ~2 equiv/αβ, and the resulting sample exhibited 0.6 spin/αβ B_{red} and 0.25 spin/αβ C_{red1}. According to our titrations, only ~1 equiv/αβ should have been required for that titration. They proposed that ACS contains another redox site called X that was responsible for consuming the extra reducing equivalents. However, Shin et al. (*35*) noticed that dithionite-reduced ACS spontaneously oxidizes over time, and for this reason, they froze their samples relatively quickly after reduction. In contrast, Seravalli et al. incubated their samples for ~1 h before freezing (*16*). Thus, another possibility for why their titration required twice the number of reducing equivalents predicted by our model is that their samples "spontaneously" oxidized during the lengthy incubation. The lack of conversion from C_{red1} to C_{red2} in their samples is consistent with this explanation (*9*, *13*).

Seravalli et al. (*16*) also titrated ACS with CO under an Ar atmosphere. In this case, the reduction process was qualitatively identical to what we observed ($B_{ox} \rightarrow B_{red}$ followed by $C_{red1} \rightarrow C_{red2}$ and $A_{ox} \rightarrow A_{red}$−CO). However, the number of equivalents per αβ required for these changes was substantially greater than that predicted by our model. Their sample (which we estimate to be 0.4−0.6 equiv/αβ reduced relative to the fully oxidized ideal state) required more than 4 equiv/αβ of CO before the A-cluster started to be reduced. According to our results, only 2.2 equiv/αβ is required before the A-cluster starts to reduce, a difference of ~2 equiv/αβ. Their titrations appear to have been performed with a gas phase present, into which some of the CO that was added would have equilibrated (we performed our titration in cuvettes devoid of a gas phase). If Seravalli et al. (*16*) did not correct for this partitioning (and they make no mention of doing so), additional reducing equivalents would have been required to achieve the same level of reduction achieved in our gas-phase-free titrations. In this case, their data would not provide evidence for another redox site.

Mechanistic Implications. Although our data discount the possibility of an additional redox site in ACS (in the redox region reliably probed by our titrations), the need for such a site remains. When reductant-free ACS (in the [C_{red1} B_{ox}] state) is reduced by CO, the resulting [C_{red2} B_{red}] state is $3e^-$ more reduced than the starting state (*9*). Since CO is a two-electron reductant, another $n = 1$ redox site (X) seems to be required. When ACS in the [C_{red1} B_{ox}] state is reduced by CO, it first converts to the [C_{red2} B_{ox}] state, and then slowly to the [C_{red2} B_{red}] state (*41*). If C_{red2} slowly reduces $B_{ox} \rightarrow B_{red}$, the resulting state would have the C-cluster poised in the hypothetical C_{int} state which should not be able to be reduced by CO. An $n = 1$ redox site X seems to require rapid oxidation of C_{int} back to C_{red1} so that C_{red1} could rapidly react with another CO and afford the observed [C_{red2} B_{red}] state. This predicament can be resolved by assuming that X is another molecule. Under in vitro conditions using pure ACS, X would be another ACS molecule in the [C_{red1} B_{ox}] state. Under in vivo conditions, X might be another protein

functionally associated with ACS.

Conclusions. Within the potential region probed by these titrations (−0.2 to −0.45 V), we conclude that there are no additional redox sites besides the A-, B-, and C-clusters. There are additional redox sites with potentials of more than −0.2 V, though these are probably nonfunctional and reflect oxidative damage. There may be additional redox sites with potentials of less than −0.45 V, but such sites were not probed by these titrations. The metal centers in the enzyme exhibit redox- and spin-state heterogeneity, causing the observed low EPR spin intensities.

SUPPORTING INFORMATION AVAILABLE

Tables of theoretical and best-fit parameters using the total-minus-X and total-plus-X models. This material is available free of charge via the Internet at http://pubs.acs.org.

REFERENCES

1. Ragsdale, S. W., and Kumar, M. (1996) *Chem. Rev. 96*, 2515−2539.
2. Xia, J., Sinclair, J. F., Baldwin, T. O., and Lindahl, P. A. (1996) *Biochemistry 35*, 1965−1971.
3. Shin, W., and Lindahl, P. A. (1992) *J. Am. Chem. Soc. 114*, 9718−9719.
4. Shin, W., and Lindahl, P. A. (1992) *Biochemistry 31*, 12870−12875.
5. Xia, J., and Lindahl, P. A. (1996) *J. Am. Chem. Soc. 118*, 483−484.
6. Russell, W. K., Stålhandske, M. V., Xia, J., Scott, R. A., and Lindahl, P. A. (1998) *J. Am. Chem. Soc. 120*, 7502−7510.
7. Xia, J., Hu, Z., Popescu, C. V., Lindahl, P. A., and Münck, E. (1997) *J. Am. Chem. Soc. 119*, 8301−8312.
8. Russell, W. K., and Lindahl, P. A. (1998) *Biochemistry 37*, 10016−10026.
9. Lindahl, P. A., Münck, E., and Ragsdale, S. W. (1990) *J. Biol. Chem. 265*, 3873−3879.
10. Lindahl, P. A., Ragsdale, S. W., and Münck, E. (1990) *J. Biol. Chem. 265*, 3880−3888.
11. Anderson, M. E., DeRose, V. J., Hoffman, B. M., and Lindahl, P. A. (1993) *J. Am. Chem. Soc. 115*, 12204−12205.
12. Anderson, M. E., and Lindahl, P. A. (1994) *Biochemistry 33*, 8702−8711.
13. Anderson, M. E., and Lindahl, P. A. (1996) *Biochemistry 35*, 8371−8380.
14. Hu, Z. G., Spangler, N. J., Anderson, M. E., Xia, J. Q., Ludden, P. W., Lindahl, P. A., and Münck, E. (1996) *J. Am. Chem. Soc. 118*, 830−845.
15. Barondeau, D. P., and Lindahl, P. A. (1997) *J. Am. Chem. Soc. 119*, 3959−3970.
16. Seravalli, J., Kumar, M., Lu, W.-P., and Ragsdale, S. W. (1997) *Biochemistry 36*, 11241−11251.
17. Maupin-Furlow, J., and Ferry, J. G. (1996) *J. Bacteriol. 178*, 6849−6856.
18. Shin, W., Anderson, M. E., and Lindahl, P. A. (1993) *J. Am. Chem. Soc. 115*, 5522−5526.
19. Shin, W., and Lindahl, P. A. (1993) *Biochim. Biophys. Acta 1161*, 317−322.
20. Lowe, D. J. (1978) *Biochem. J. 175*, 955−957.
21. Roberts, L. M., and Lindahl, P. A. (1994) *Biochemistry 33*, 14339−14349.
22. Roberts, L. M., and Lindahl, P. A. (1995) *J. Am. Chem. Soc. 117*, 2565−2572.
23. Ragsdale, S. W., Clark, J. E., Ljungdahl, L. G., Lundie, L. L., and Drake, H. L. (1983) *J. Biol. Chem. 258*, 2364−2369.
24. Raybuck, S. A., Bastian, N. R., Orme-Johnson, W. H., and Walsh, C. T. (1988) *Biochemistry 27*, 2698−2702.
25. Pelley, J. W., Garner, C. W., and Little, G. H. (1978) *Anal. Biochem. 86*, 341−343.
26. Budavari, S., O'Neil, M. J., Smith, A., and Heckelman, P. E. (1989) *The Merck Index*, 11th ed., p 533, Merck & Co., Inc., Rahway, NJ.
27. Altman, T. E. (1981) Analysis of Nuclear Quadrupole Coupling in EPR Spectra, Ph.D. Dissertation, University of Illinois at Urbana−Champaign, Urbana, IL.
28. Belford, R. L., and Nilges, M. J. (1979) Computer Simulation of Powder Spectra EPR Symposium, 21st Rocky Mountain Conference, August 1979, Denver, CO.
29. Nilges, M. J. (1981) Electron Paramagnetic Resonance Studies of Low Symmetry Nickel I and Molybdenum V Complexes, Ph.D. Dissertation, University of Illinois at Urbana−Champaign, Urbana, IL.
30. Dubila, E. P. (1983) Studies of Nuclear Quadrupole Effects in Transition Metal Complexes by Electron Paramagnetic Resonance, Ph.D. Dissertation, University of Illinois at Urbana−Champaign, Urbana, IL.
31. Orme-Johnson, N. R., and Orme-Johnson, W. H. (1978) *Methods Enzymol. 52*, 252−257.
32. Moore, S., and Stein, W. H. (1963) *Methods Enzymol. 6*, 819−831.
33. Godel, H., Seitz, P., and Verhoef, M. (1992) *LC·GC International 5*, 44−49.
34. Reiger, P. H. (1994) *Electrochemistry*, Chapman & Hill, New York.
35. Shin, W., Stafford, P. R., and Lindahl, P. A. (1992) *Biochemistry 31*, 6003−6010.
36. Menon, S., and Ragsdale, S. W. (1996) *Biochemistry 35*, 12119−12125.
37. Liu, K., Valentine, A. M., Wang, D. L., Huynh, B. H., Edmondson, D. E., Salifoglou, A., and Lippard, S. J. (1995) *J. Am. Chem. Soc. 117*, 10174−10185.
38. Liu, K., Wang, D. L., Huynh, B. H., Edmondson, D. E., Salifoglou, A., and Lippard, S. J. (1994) *J. Am. Chem. Soc. 116*, 7465−7466.
39. Moenne-Loccoz, P., Baldwin, J., Ley, B. A., Loehr, T. M., and Bollinger, J. M. (1998) *Biochemistry 37*, 14659−14663.
40. Broadwater, J. A., Ai, J. Y., Loehr, T. M., Sanders-Loehr, J., and Fox, B. G. (1998) *Biochemistry 37*, 14664−146671.
41. Kumar, M., Lu, W.-P., Liu, L., and Ragsdale, S. W. (1993) *J. Am. Chem. Soc. 115*, 11646−11647.

BI990397N